substrate using potential theory," *IEEE Trans. Microwave Theory Tech.*, vol. 41, pp. 2067–2073, Dec. 1993.
[2] L B. Felsen and N. Marcuvitz, *Radiation and Scattering of Waves*. New York: IEEE, 1994.
[3] K A. Michalski, "Formulation of mixed-potential integral equations for arbitrarily shaped microstrip structures with uniaxial substrate," *J. Electromagn. Waves Applicat.*, vol. 7, pp. 899–917, 1993.
[4] J. C Goswami, "Applications of semi-orthogonal spline wavelets in electromagnetics and microwave problems," Ph D dissertation, Texas A&M Univ., College Station, TX, Aug. 1995
[5] T. S Horng, N. G. Alexópoulos, S. C Wu, and H Y. Yang, "Full-wave spectral-domain analysis for open microstrip discontinuities of arbitrary shape including radiation and surface-wave losses," *Int. J. Microwave Millimeter-Wave Computer-Aided Eng*., vol. 2, pp 224–240, 1992.
[6] A K. Bhattacharyya, "Approximate formulae for the surface wave numbers in a grounded dielectric structure," *Microwave Opt. Technol Lett*., vol. 3, pp 169–172, 1990
[7] C I. G. Hsu, R F Harrington, and K A Michalski, "On the mode spectrum of a parallel-plate waveguide filled with a two-layer uniaxial medium," *Microwave Opt Technol. Lett.*, vol. 5, pp 318–321, 1992.
[8] J. R. Mosig, "Integral equation technique," in *Numerical Techniques for Microwave and Millimeter-Wave Passive Structures*, T Itoh Ed., New York: Wiley, 1989, pp. 133–213.
[9] G. Gronau and I. Wolff, "A simple broad-band device de-embedding method using and automatic network analyzer with time-domain option," *IEEE Trans. Microwave Theory Tech.*, vol. 37, pp. 479–483, Mar. 1989.
[10] R. E. Collin, private communication.

Development of Accurate On-Wafer, Cryogenic Characterization Techniques

J. Laskar, J. J. Bautista, M. Nishimoto, M. Hamai, and R. Lai

***Abstract*— Significant advances in the development of high electron mobility field-effect transistors (HEMT's) have resulted in cryogenic, low-noise amplifiers (LNA's) whose noise temperatures are within an order of magnitude of the quantum noise limit ($h\nu/k$). Further advances in HEMT technology at cryogenic temperatures may eventually lead to the replacement of maser and superconducting-insulator-superconducting (SIS) front-ends in the 1–100 GHz frequency band. Key to identification of the best HEMT's and optimization of cryogenic LNA's is accurate and repeatable device measurements at cryogenic temperatures. A cryogenic on-wafer noise and scattering parameter measurement system has been developed to provide a syst**

ematic investigation of HEMT noise characteristics. In addition, an improved parameter extraction technique has been developed to help understand the relationship between device structure and LNA performance.

I. Introduction

As the demands for high performance satellite transmit/receive components increase, researchers have looked for viable alternatives to increase signal to noise margins at higher frequencies. Notable results have included the development of cryogenic low-noise amplifiers at X- and Ka-bands [1], [2] and the development of hybrid high temperature superconductor and semiconductor components [3]. The improvement of high performance satellite links and the need for high performance light satellites has provided the impetus for continued development and understanding of cryogenic microwave components. A critical element in the application of this technology is the development of a robust on-wafer characterization technique at cryogenic temperatures.

In recent years, significant progress has been made in the development of cryogenic, on-wafer probing systems [4]–[10]. The major shortcoming of previous efforts has been the lack of a repeatable and accurate system yielding results comparable to room temperature systems.

In this paper, we report a quantitative investigation in the accuracy of on-wafer cryogenic noise and S-parameter measurements. Results shown in this paper include:

1) demonstration of two-tier cryogenic calibrations;
2) study of the effect of temperature on calibration repeatability;
3) development of improved parameter extraction techniques for cryogenic temperatures;
4) investigation of room temperature noise techniques applied at cryogenic temperatures;
5) initial results of an on-chip cryogenic noise technique.

II. Cryogenic-Probe Measurement System

A variety of test fixtures have been used [4]–[9] to evaluate HEMT performance from 300 K to 15 K. Most of these fixtures are similar to the one developed by Liechti and Larrick [10], a microwave test fixture that could be immersed in liquid nitrogen. To date, it has been difficult to make broad band scattering (S)-parameter measurements in such an environment due to the limited accuracy of the full two-port calibrations.

The cryogenic microwave system in this work uses coplanar waveguide probes in a vacuum station coupled to a vector network analyzer for scattering parameter measurements, and a noise and test set with a noise system for microwave noise parameter measurements. The microwave measurement system currently under development incorporates measurement tools originally developed for the first system in 1989 [11], [12]. The cryogenic probe measurement system contains ports for RF cables, thermometers, vacuum pumps, dry nitrogen backfill lines, coplanar probes with manipulators, and a closed-cycle refrigerator cold head. The probe body rests on a copper block attached to a fiberglass post. The fiberglass reduces the thermal load and copper braiding from the cold head thermally anchors the probe to the 12 K cold station assuring sample temperatures of 12–20 K. The mechanical and thermal stability of the wafer stage is established by supporting it on fiberglass posts above the cold head and thermally anchoring it to the cold station with flexible copper braids.

The most important feature of this design is the incorporation of a closed-cycle helium refrigeration system. The first successful designs of on-wafer cryogenic systems used open-cycle cooling to reduce start up costs and avoid mechanical vibrations. However, for long term temperature stability, a closed-cycle helium source provides the optimum solution. Decoupling and damping of the vibrations from the cold head to the probe station is accomplished with a bellows and vibration mount. This system allows small-signal microwave measurements from DC to 40 GHz over a physical temperature range of 16–300 K. Since the microwave hardware is insulated by vacuum

Manuscript received September 22, 1995; revised March 20, 1996

J. Laskar is with the Georgia Institute of Technology, School of Electrical and Computer Engineering, Atlanta, GA 30332-0250 USA.
J. J. Bautista is with Jet Propulsion Laboratory, California Institute of Technology, Pasadena, CA 91109-8099 USA.
M. Nishimoto, M Hamai, and R. Lai are with TRW Electronics Systems and Technology Division, Redondo Beach, CA 90278 USA.

Publisher Item Identifier S 0018-9480(96)04728-X.

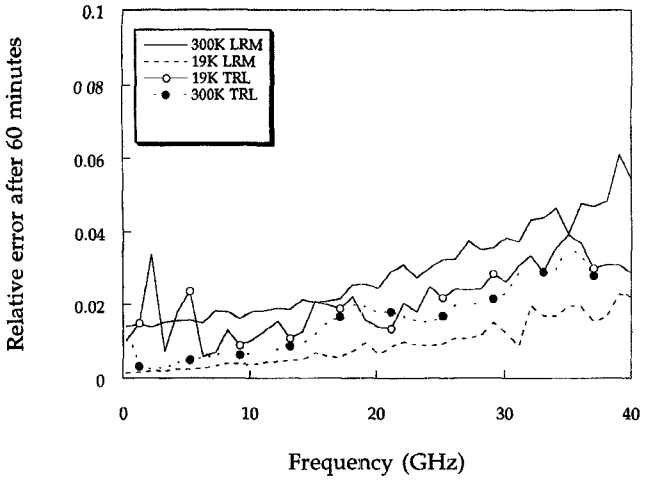

Fig. 1. Relative error between two successive S-Parameter measurements collected at 1 hour intervals at 300 K and 19 K.

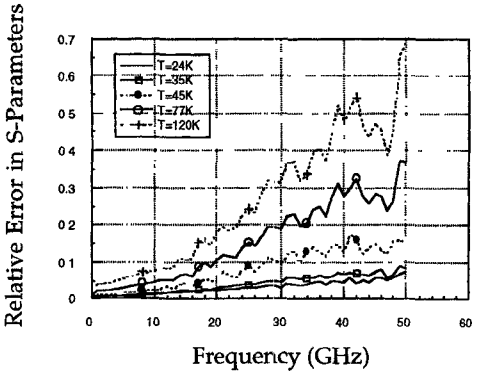

Fig. 2. Effect of sample temperature variation on worst case vector error using a two-tier LRM calibrations. The first calibration is performed at 24 K and subsequent calibrations are performed at higher temperatures.

there is no frost buildup or large thermal gradients, resulting in a system that is accurate, reliable and flexible.

III. Calibration Considerations

Two key elements in performing two-port microwave measurements are stability of error terms and accuracy, by establishing a known electrical reference plane. The measurement accuracy is directly related to the calibration conditions. Thermal gradients across the gold plated ceramic probe tips and coax to coplanar transitions [13] alter the electrical characteristics of the measurement lines. The process of cooling the sample in the laboratory can also produce changes in the calibration. The network analyzer typically requires a new calibration if the ambient laboratory temperature varies by greater than $\pm 1°C$. The proximity of the cooled probe system to the network analyzer can change the ambient environment (both temperature and humidity). The combined results of these effects are appreciable errors in cryogenic temperature measurements.

In order to demonstrate that our system errors are stable, we performed LRM and TRL calibrations an hour apart at both 19 K and 300 K. Calibrations at each temperature are compared using a method developed by NIST [14], which demonstrates repeatability of calibrations. The results, see Fig. 1, show comparable calibration repeatability at both 19 K and 300 K. The 19 K results compare favorably with the best room temperature results obtained by NIST [15].

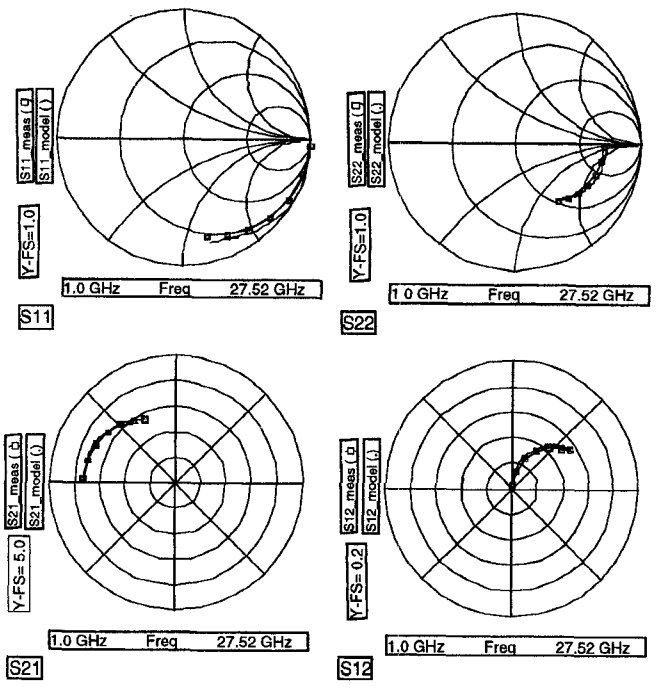

Fig. 3. Demonstration of agreement between measured and modeled S-parameters at cryogenic temperatures. The extracted parameters were obtained via measurement and not circuit optimization techniques.

In Fig. 2, we demonstrate the effect of temperature upon calibration stability. In this case, the first calibration is performed at 24 K and subsequent calibrations are performed at higher temperatures. Since all calibrations are performed within one hour, the higher error functions observed in Fig. 2 are due to the temperature variation within the measurement chamber and not drift in the network analyzer. These results emphasize that to achieve repeatable cryogenic S-parameters one must:

1) provide a stable thermal environment;
2) perform calibrations at the temperature of interest.

An accurate cryogenic, two-port calibration for S-parameter measurements must satisfy several criteria. At room temperature we can typically find that return loss in the transmission through standard should be better than -45 dB and the insertion loss should vary within ± 0.1 dB of 0 dB. Next, the calibrated open standard is found to be within ± 0.1 dB of 0 dB. Our cryogenic calibrations satisfy these criteria. A qualitative verification can be performed by evaluating additional representative elements not used in the calibration sequence.

The solution to maintaining calibration integrity and achieving low sample temperatures is to thermally anchor the probe body and perform cryogenic calibrations. By thermally anchoring the probe to the cold head at 12 K, the thermal load to the DUT is minimized. The remaining microwave hardware (connectors, cables and input to ANA) are thermally isolated via vacuum and stainless steel hardware. The thermally anchored probe can be calibrated at specific temperatures during a measurement cycle. This eliminates the problem of calibration error and allows accurate correlation of DUT temperature and measured characteristics.

The most accurate and repeatable method of measuring noise parameters at cryogenic temperatures is to place the impedance generator within a wavelength of the DUT input. The equivalent noise temperature of the noise source must also be comparable to the DUT noise temperature. This approach would require development of a cryogenic noise generator and noise source.

TABLE I
EXTRACTED SMALL-SIGNAL ELEMENT VALUES AT 300 K AND 16 K USING MODIFIED HOT/COLD FET EXTRACTION

PHEMT	300K	16K
Lg (pH)	28.3	39.4
Ld (pH)	27.2	44.6
Ls (pH)	4.6	3.8
Rg (ohms)	15.3	12.4
Rd (ohms)	3.4	4.0
Rs (ohms)	0.6	0.8
Cpg (fF)	7.5	6.5
Cpd (fF)	3.2	12.2

InP HEMT	300K	16K
Lg (pH)	13.5	23.8
Ld (pH)	4.5	25.5
Ls (pH)	0.3	0.2
Rg (ohms)	18.5	4.6
Rd (ohms)	4.6	1.0
Rs (ohms)	1.2	0.3
Cpg (fF)	1.2	1.1
Cpd (fF)	1.4	1.1

MODIC FET	300K	16K
Lg (pH)	30.6	31.0
Ld (pH)	28.2	38.0
Ls (pH)	1.6	1.1
Rg (ohms)	12.4	9.9
Rd (ohms)	3.2	4.6
Rs (ohms)	0.7	0.9
Cpg (fF)	21.0	19.6
Cpd (fF)	10.0	17.8

For this initial investigation of on-wafer noise parameter measurements at cryogenic temperatures only the probe tips are cooled while the impedance state generator and solid state noise source (both commercially available) are kept at room temperature (several wavelengths away from the DUT). In this configuration the input losses introduce noise comparable to or greater than the noise of the device under test (DUT) and reduces the range of available impedance states. For example, in the frequency range of 2–18 GHz for cryogenic temperatures the worst case noise temperature error is ± 25 K, while device noise temperatures are typically under 10 K. Although this configuration does not provide accurate single frequency noise parameter measurements, it does provide for fast and efficient broadband (2–18 GHz) on-wafer measurements.

IV. PARAMETER EXTRACTION TECHNIQUES

A variety of HEMT structures have been investigated to determine the temperature behavior of both the intrinsic and extrinsic device parameters. The structures investigated include: AlGaAs/GaAs HEMT (conventional), AlGaAs/InGaAs pseudomorphic HEMT (PHEMT) and lattice matched InAlAs/InGaAs HEMT (InP HEMT).

An HEMT parasitic model has been developed based upon the results in [16]–[19]. This model accounts for bias dependent resistances which affect the parasitic resistances (R_s, R_g, and R_d) as a function of gate-source bias with $V_{ds} = 0$ V. The intrinsic and extrinsic parameters can be extracted using the equations presented by [16], conventional Hot/Cold FET techniques and the basic model in [19]. One major modification has been the removal of the depletion capacitance cited in [19] resulting in a symmetric parasitic model.

This Hot/Cold FET analysis has been applied to several different HEMT structures. We demonstrate excellent agreement between measured and model data at cryogenic temperatures as shown in Fig. 3. A summary of typical results for the conventional, PHEMT and InP HEMT are shown in Table I. Table II shows the results including the small-signal model elements for the InP HEMT at various temperatures. The InP HEMT shows the greatest variation with temperature, primarily due to a higher electron mobility. Two of the most important parameters for extraction are the source resistance, R_s, and inductance, L_s. These terms must be accurately extracted since they serve as a feedback term in device operation.

V. MEASUREMENT RESULTS

Scattering parameters were measured from 1–25 GHz, while noise parameter measurements were attempted from 2–18 GHz for the same bias and temperature conditions. For the experimental conditions all the S-parameters were measured with an error of less than 2% between measured and modeled data. The development of an accurate HEMT device model allows us to predict the behavior of Γ_{opt} and $T_{\min}$ as a function of frequency. Based upon the direct measurement of the cryogenic noise parameters, cryogenic S-parameters and the room temperature device model we can extract a complete temperature dependent device model. We directly measure the noise parameters at cryogenic temperatures and correlate with the predicted performance based upon the model presented in [20]. All four noise parameters could not be reliably measured for the physical temperature and frequency spans of interest. In Fig. 4, we demonstrate the variation of noise temperatures as a function of bias at cryogenic temperatures. At cryogenic temperatures, however, because of the lossy input and long electrical distance of the impedance generator from the device input only the minimum noise temperature was reliably determined above 8 GHz. For frequencies above 8 GHz the percentage error in the minimum noise temperature was determined to be less than 25%. The resulting measurements were then fit to a straight line. The fitting error varied from 6–11%. Fig. 5 shows a plot of the measured minimum noise temperature as function of percentage drain to source saturation current at 18 GHz at two physical temperatures, 11 and 16 K. At these two temperatures the rms error in the minimum noise temperature was ± 12 K and ± 6 K, respectively.

VI. ANALYSIS AND DISCUSSION

The pioneering work of Weinreb and Pospieszalski [21], [22] has led to the development of HEMT based LNA's which are the lowest noise transistor circuits produced to date. These impressive results have been achieved without the benefit of cryogenic, broad band noise measurements. Pospieszalski's method relies on dc cryogenic measurements (g_m and r_{ds}), manufacturer's or measured room temperature broad band S-parameter data (remaining circuit elements), and a single frequency cryogenic, noise parameter measurement (T_d and T_g) to determine all of the circuit parameters for his empirical noise model.

For the Pospieszalski noise model [20], the measured noise parameters are required to determine T_d, the equivalent drain temperature associated with g_{ds}, and the equivalent gate temperature T_g associated with r_{gs} and as an additional check on the intrinsic element values. Pospieszalski [23] found, that for a variety of different HEMT and FET devices T_g was equal to the ambient temperature for I_{ds} less than 20 mA. T_d on the other hand is strongly dependent on I_{ds} and within measurement error a single function may describe its dependence for all devices. (At room temperature using on-wafer

TABLE II
EXTRACTED ELEMENTS FOR THE DIFFERENT PHYSICAL TEMPERATURES AND BIAS SETTINGS

I_{dss}, %	I_{dss}, mA	L_d, pH	L_g, pH	L_s, pH	R_d, Ω	R_g, Ω	R_s, Ω	C_{ds}, fF	C_{gd}, fF	C_{gs}, fF	G_m, ms	R_{ds}, Ω	R_{gs}, Ω	R_t Ω	T_d, K	T_{min}/f, K/GHz
							T_{phys} = 11 K									
15	2.9	4	15	4	5.0	3.8	1.00	17.20	22.90	76.50	39.70	576.70	1.00	5.80	234	0.123
25	4.7	4	15	4	4.6	3.8	1.00	17.40	22.20	84.30	50.30	450.00	1.00	5.80	373	0.153
50	9.6	4	15	4	4.7	3.5	1.00	17.30	21.60	91.40	65.00	370.00	1.00	5.50	750	0.196
75	14.9	4	15	4	6.7	3.0	1.00	18.80	21.20	92.20	72.00	344.20	0.70	4.70	1158	0.212
100	18.7	4	15	4	6.0	3.0	1.00	19.00	19.72	103.00	72.00	331.80	1.50	5.50	1451	0.292
							T_{phys} = 16 K									
15	2.4	4	15	4	6.0	3.0	2.00	18.80	31.10	68.60	36.25	589.00	2.00	7.00	201	0.147
25	3.9	4	15	4	6.0	3.0	1.00	17.00	31.00	71.00	45.30	480.00	2.00	6.00	316	0.157
50	8.4	4	15	4	6.0	2.0	1.00	17.90	30.40	78.70	60.90	368.00	2.00	5.00	663	0.195
75	12.7	4	15	4	6.0	3.0	1.00	15.70	30.10	80.80	68.50	344.80	2.00	6.00	994	0.247
100	16.4	4	15	4	6.0	3.0	2.30	17.60	25.50	123.60	67.00	303.00	2.00	7.30	1279	0.515
							T_{phys} = 36 K									
15	2.5	4	15	4	6.0	3.0	2.27	22.25	24.77	72.19	35.07	625.75	11.21	16.48	229	0.381
25	4.1	4	15	4	6.0	3.0	2.27	21.42	24.41	80.78	47.44	469.76	7.92	13.19	352	0.403
50	8.3	4	15	4	6.0	3.0	2.27	21.88	23.39	92.24	64.56	352.77	6.00	11.27	675	0.500
75	12.5	4	15	4	6.0	3.0	2.27	15.47	29.67	90.21	74.60	298.41	5.50	10.77	999	0.547
100	16.4	4	15	4	6.0	3.0	2.27	16.91	24.56	133.61	66.91	303.99	5.50	10.77	1299	1.021
							T_{phys} = 49 K									
15	2.2	4	15	4	6.0	3.0	2.27	21.83	24.93	72.19	35.42	526.80	10.88	16.15	218	0.464
25	3.7	4	15	4	6.0	3.0	2.27	21.51	24.39	71.92	47.40	468.31	7.20	12.47	334	0.398
50	7.5	4	15	4	6.0	3.0	2.27	21.88	23.39	92.24	64.56	352.77	6.00	11.27	627	0.562
75	11.1	4	15	4	6.0	3.0	2.27	20.65	23.06	96.51	72.77	324.14	6.00	11.27	904	0.654
100	15.8	4	15	4	6.0	3.0	2.27	21.69	17.45	137.63	66.24	315.41	6.00	11.27	1266	1.229
							T_{phys} = 300 K									
15	2.7	4	15	4	6.0	3.1	3.40	17.10	19.50	69.60	28.13	798.00	2.00	8.50	508	1.253
25	4.6	4	15	4	6.0	3.0	4.90	19.30	18.33	83.60	40.36	560.00	2.00	9.90	654	1.533
50	9.1	4	15	4	6.0	1.5	3.40	18.70	18.02	90.00	51.00	464.90	2.00	6.90	1001	1.480
75	13.8	4	15	4	6.0	3.0	3.50	18.40	17.41	96.60	57.90	417.70	2.00	8.50	1363	1.912
100	18.4	4	15	4	6.0	1.96	3.70	18.24	17.05	101.60	60.40	398.30	2.00	7.66	1717	2.104

noise and scattering parameters from 4–18 GHz Pospieszalski used measured and modeled values for the intrinsic R_{opt} and $T_{\min}$ using a least squares fit to arrive at values of T_d and T_g.)

Ideally for low noise device studies and circuit modeling it is preferable to have both broadband measured noise and scattering parameters. Since only the measured minimum noise temperatures were obtained, only the predicted and measured noise temperatures as a function of drain currents (I_{ds}) at 18 GHz for a variety of different temperatures are compared. The predicted minimum noise temperature is calculated using Pospieszalski's expression

$$T_{\min} = \frac{2\pi f C_{gs}\sqrt{g_{ds} r_t T_g T_d}}{g_m}$$

for the minimum noise temperature. The small signal circuit elements are those extracted from the measured s-parameters while T_g is the device physical temperature and T_d is estimated from the results in [23].

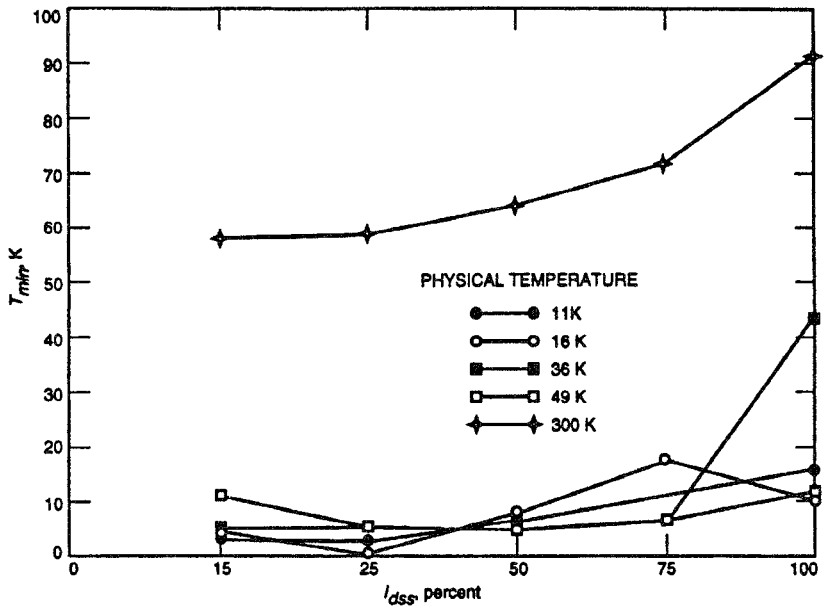

Fig. 4. Measured noise temperature at 18 GHz and several temperatures.

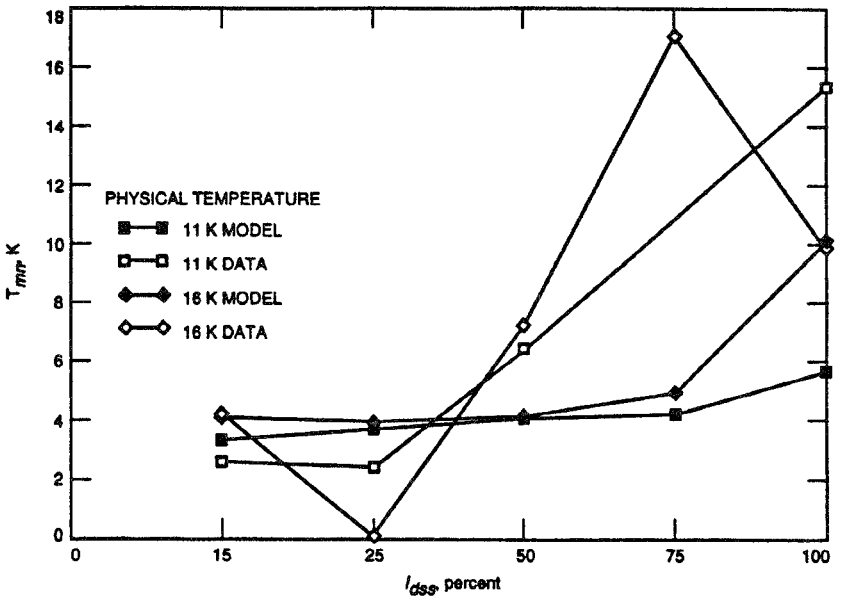

Fig. 5. Comparison of measured and modeled $T_{\min}$ at 11 K and 16 K at 18 GHz.

For single frequency measurements at 18 GHz the worst case error for the measured minimum noise temperature is ± 25 K and ± 15 K for the calculated model value. That there is agreement with the cryogenic results indicates that a closer examination with a more accurate and reliable method of cryogenic noise parameter measurement and small-signal element extraction technique is absolutely necessary. Toward this goal we have begun development of a coolable noise and impedance generator, integrated with the cryogenic, microwave probe for broadband scattering and noise parameter measurements.

VII. Conclusion

The feasibility of cryogenic, broadband on-wafer scattering and noise parameter measurements for the systematic investigation of HEMT noise characteristics has been demonstrated. In addition, an improved parameter extraction technique has been developed to help understand the relationship between device structure and LNA performance.

Future development of a coolable noise and impedance generator, integrated with the cryogenic, microwave probe will be capable of performing broadband scattering and noise parameter measurements. The development of a cryogenic probe tip integrated with a cryogenic noise and impedance generator capable of performing both scattering and noise parameter measurements will circumvent the limitations posed by the current characterization techniques. An integrated probe will enhance the fundamental study of noise sources in solid state technology and lead to improved cost and performance benefits for HEMT cryogenic technology.

References

[1] K. H. G. Duh *et al.*, "32 GHz cryogenically cooled HEMT low-noise amplifiers," *IEEE Trans. Electron Devices*, vol. 36, pp. 1528–1534, 1989

[2] M. Pospiezalski *et al.*, "Very low noise and low power operation of cryogenic AlInAs/GaInAs/InP HFET's," in *IEEE MTT-S Dig.*, 1994, pp. 1345–1346.

[3] K. B. Bhasin *et al.*, "Performance of a YBaCuO superconducting filter/GaAs low noise amplifier hybrid circuit," in *IEEE MTT-S Dig.*, 1992, pp. 481–483.
[4] W. Brockerhoff *et al.*, "RF measurements and characterization of heterostructure field-effect transistors at low temperatures," *IEEE Trans. Microwave Theory Tech.*, vol. 37, pp. 1380–1388, 1989.
[5] V. Iyengar *et al.*, "Low-temperature current drift and its origin in heterostructure and quantum-well MODFET's," in *Proc. 14th Gallium Arsenide Related Compounds*, 1988, pp. 669–672.
[6] J. Kolodzey *et al.*, "Cryogenic temperature performance of modulation-doped field-effect transistors," *Electronic Lett.*, vol. 25, pp. 777–779, 1989.
[7] R. Lai *et al.*, "Characteristics of 0.8- and 0.2-μm gate length $In_xGa_{1-x}As/In_{0.52}Al_{0.48}As/InP$ modulation-doped field-effect transistors at cryogenic temperatures," *IEEE Trans. Electron Devices*, vol. 39, pp. 2206–2213, 1992.
[8] J. W. Smuk, M. G. Stubbs, and J. S Wight, "Vector measurements of microwave devices at cryogenic temperatures," in *IEEE MTT-S Dig.*, 1989, pp. 1195–1198.
[9] Y. Kwark, P. Solomon, and D. La Tulipe, "S-parameter characterization of GaAs gate SISFET's at liquid nitrogen temperatures," in *Proc. IEEE/Cornell Univ. Conf. Advanced Concepts High Speed Dev. Ckts.*, pp. 208–217, 1989.
[10] C. A. Leichti and R. B. Larrick, *IEEE Trans. Microwave Theory Tech.*, vol. MTT-24, pp. 365–370, June 1976.
[11] J. Laskar and J. Kolodzey, "Cryogenic vacuum high frequency probe station," *J. Vac. Sci. Technol.*, vol. B, no. 8, pp. 1161–1165, Sept./Oct. 1990.
[12] J. Laskar and M. Feng, "An on-wafer cryogenic microwave probing system for advanced transistor and superconductor applications," *Microwave J.*, vol. 36, pp. 104–114, Feb. 1993.
[13] H. Meschede *et al.*, "On-wafer microwave measurement setup for investigations on HEMT's and high-T_c superconductors at cryogenic temperatures down to 20 K," *IEEE Trans. Microwave Theory Tech.*, vol. 40, pp. 2325–2331, 1992.
[14] R. B. Marks, "A multiline method of network analyzer calibration," *IEEE Trans. Microwave Theory Tech.*, vol. 39, pp. 1205–1215, 1991.
[15] D. F. Williams and R. B. Marks, "Accurate transmission line characterization," *IEEE Microwave Guided Wave Lett.*, vol. 3, pp. 247–249, 1993.
[16] M. Golio, W. Seely, and D. Halchin, "Spreadsheet program extracts transistor parasitic elements," *Microwaves RF*, pp. 67–73, Oct. 1992.
[17] M. Berroth and R. Bosch, "Broad-band determination of the FET small-signal equivalent circuit," *IEEE Trans. Microwave Theory Tech.*, vol. 38, no. 7, pp. 891–895, 1990.
[18] G. Dambrine *et al.*, "A new method for determining the FET small-signal equivalent circuit," *IEEE Trans. Microwave Theory Tech.*, vol. 36, no. 7, pp. 1151–1159, 1988.
[19] P. White and R. M. Healy, "Improved equivalent circuit for determination of MESFET and HEMT parasitic capacitances from 'Coldfet' measurements," *IEEE Microwave Guided Wave Lett.*, vol. 3, no. 12, pp. 453–454, Dec. 1993.
[20] M. Pospiezalski, "Modeling of noise parameters of MESFET's and MODFET's and their frequency and temperature dependence," *IEEE Trans. Microwave Theory Tech.*, vol. 37, pp. 1340–1350, 1989.
[21] S. Weinreb, R. Harris, and M. Rothman, "Millimeter-wave noise parameters of high-performance HEMT's at 300 K and 17 K," in *IEEE MTT-S Dig.*, 1989, pp. 813–816.
[22] M. W. Pospieszalski, "Cryogenically-cooled, HFET amplifiers and receivers: State-of-the-art and future," in *IEEE MTT-S Dig.*, 1992, pp. 1369–1372.
[23] M. W. Pospieszalski and A. C. Niedzwiecki, "FET noise model and on-wafer measurement of noise parameters," in *IEEE MTT-S Dig.*, 1991, pp. 1117–1122.

Radial Mode Matching Analysis of Ridged Circular Waveguides

Uma Balaji and Ruediger Vahldieck

***Abstract*—In this paper a radial mode matching analysis is presented to calculate rigorously the TE and TM mode propagation in single- double-, triple-, and quadruple-ridged circular waveguide structures. The ridges have been cut radially in all the cases. Results are presented for variations of the ridge depth and ridge thickness and are compared to results from finite element analysis. Furthermore, for the first time, the characteristic impedance of the double and quadruple-ridged circular waveguides have been calculated using the power-voltage definition.**

I. Introduction

Various numerical techniques have been applied in the past to solve the eigenvalue problem of single- [1], double- [2]–[4], triple- [5], [6], and quadruple-ridged [4], [7], [8] circular waveguides with ridges of uniform thickness or ridges that are radially cut. Most of the above work is based on the discretization of the space or space and time to solve the Helmholtz equation. To avoid memory consuming space discretization techniques, a radial mode matching method has been developed [14] for the analysis of single- and double-ridged circular waveguides. The method is extended here to triple- and quadruple-ridged circular waveguides. In order to avoid mixed coordinate systems which occur when rectangular ridges are utilized in a cylindrical waveguide, the ridges are assumed to be conically shaped [10]. Mechanically, they are as simple to fabricate as the more traditional rectangular ridges. The approach developed in the following is rigorous and can be applied to symmetrical as well as asymmetrical structures.

II. Theory

1) Eigenvalue Problem: To start with we first consider the cross section of the single-ridged circular waveguide of Fig. 1(a) and (b). The double- and quadruple-ridged circular waveguide can be easily derived from the following theory by considering electric wall (ew) and magnetic wall (mw) symmetry. The eigenvalues of the orthogonal dominant modes and higher order modes of such a structure can be obtained from the solution of the Helmholtz equation in cylindrical coordinates.

Solving the Helmholtz equation in each homogeneous subregion and considering the boundary condition, the potential function for regions 1 and 2 for TE modes can be written as follows:

$$\psi^{(1)} = \sum_{n=r}^{N1} A_n J_n(k_c\rho) \begin{cases} \sin n\phi & r = 1 \text{ for mw} \\ \cos n\phi & r = 0 \text{ for ew} \end{cases} \tag{1}$$

$$\psi^{(2)} = \sum_{m=r}^{N2} C_m [H_l^{(2)'}(k_c b) H_l^{(1)}(k_c\rho) - H_l^{(1)'}(k_c b) H_l^{(2)}(k_c\rho)] \cdot \begin{cases} \cos l(\phi-\theta) & r = 1, 3 \text{ and } l = \dfrac{m\pi}{2(\pi-\theta)} \text{ for mw} \\ \cos l(\phi-\theta) & r = 0 \text{ and } l = \dfrac{m\pi}{\pi-\theta} \text{ for ew.} \end{cases} \tag{2}$$

Manuscript received October 3, 1995; revised March 20, 1996.

The authors are with the Department of Electrical and Computer Engineering, University of Victoria, Victoria, British Columbia, V8W 3P6 Canada.

Publisher Item Identifier S 0018-9480(96)04729-1.